Title

Immunomodulation of the NLRP3 Inflammasome through Structure-Based Activator Design and Functional Regulation via Lysosomal Rupture.

Journal

ACS central science, 4(8)

ISSN

2374-7943

Authors

Manna, Saikat
Howitz, William J
Oldenhuis, Nathan J
et al.

Publication Date

2018-08-22

Peer reviewed

ACS central science

Research Article

Cite This: ACS Cent. Sci. 2018, 4, 982−995

Immunomodulation of the NLRP3 Inflammasome through Structure-Based Activator Design and Functional Regulation via Lysosomal Rupture

Saikat Manna,[†,‡,∥] William J. Howitz,[†,∥] Nathan J. Oldenhuis,[†] Alexander C. Eldredge,[†] Jingjing Shen,[‡] Fnu Naorem Nihesh,[†,‡] Melissa B. Lodoen,[§] Zhibin Guan,[†] and Aaron P. Esser-Kahn*[,†,‡]

[†]Department of Chemistry, University of California, Irvine, Irvine, California 92697, United States

[‡]Institute for Molecular Engineering, University of Chicago, Chicago, Illinois 60637, United States

[§]Department of Molecular Biology and Biochemistry and The Institute for Immunology, University of California, Irvine, Irvine, California 92697, United States

Supporting Information

ABSTRACT: The NLRP3 inflammasome plays a role in the inflammatory response to vaccines, in antimicrobial host defense, and in autoimmune diseases. However, its mechanism of action remains incompletely understood. NLRP3 has been shown to be activated by diverse stimuli including microbial toxins, ATP, particulate matter, etc. that activate multiple cellular processes. There have been two major challenges in translating inflammasome activators into controlled adjuvants. Both stem from their chemical and structural diversity. First, it is difficult to identify a minimum requirement for inflammasome activation. Second, no current activator can be tuned to generate a desired degree of activation. Thus, in order to design such immunomodulatory biomaterials, we developed a new tunable lysosomal rupture probe that leads to significant differences in inflammasome activation owing to structural changes as small as a single amino acid. Using these probes, we conduct experiments that suggest that rupturing lysosomes is a critical, initial step necessary to activate an inflammasome and that it precedes other pathways of activation. We demonstrate that each molecule differentially activates the inflammasome based solely on their degree of lysosomal rupture. We have employed this understanding of chemical control in structure-based design of immunomodulatory NLRP3 agonists on a semipredictive basis. This information may guide therapeutic interventions to prevent or mitigate lysosomal rupture and will also provide a predictive framework for dosable activation of the NLRP3 inflammasome for potential applications in vaccines and immunotherapies.

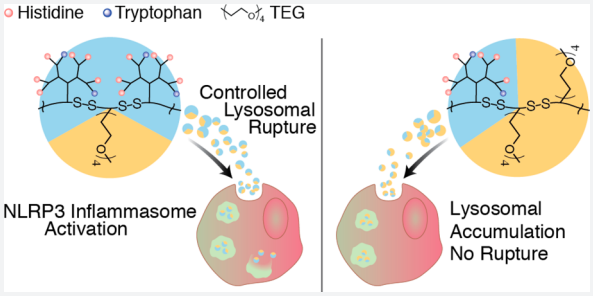

INTRODUCTION

Inflammasomes are multiprotein subunit platforms that control the formation of the catalytically active protease, caspase-1, leading to cleavage of proinflammatory cytokines interleukin-1β (IL-1β) and interleukin-18 (IL-18) followed by pyroptosis.[1,2] Although the inflammasome plays a critical role in immune activation, pathogen clearance, and adjuvant activity,[3] aberrant inflammasome activation has been implicated in various autoimmune diseases.[4] Among the inflammasomes activated by the NOD-like receptor (NLR) family, the NLRP3 inflammasome is the most well understood and widely studied owing to its role in host defense and innate immunity.[5] However, despite over a decade of studies, the precise mechanism or mechanisms of its activation remain ambiguous. Munoz-Planilo et al. have demonstrated potassium efflux as a criterion for activation of the NLRP3 inflammasome;[6] however upstream minimal determinants for NLRP3 activity have yet to be identified. What is clear is that immune cells must first be primed by a Toll-like receptor (TLR) agonist or inflammatory cytokines such as tumor necrosis factor-α (TNF-α), leading to NF-κB signaling and transcriptional priming of pro-IL-1β. After priming, the mechanism becomes less clear. The NLRP3 inflammasome has been shown to be activated by a diverse array of stimuli including ATP, pore-forming toxins like maitotoxin,[7] various crystalline and particulate matter such as alum, urea, and silica,[8] chemotherapeutic agents such as 5-fluorouracil,[9] and small peptides like Leu−Leu−OMe.[8] Each of these structurally diverse stimuli triggers multiple cellular events including membrane permeabilization, reactive oxygen species (ROS) production, lysosomal damage, mitochondrial dysfunction, and other cellular processes. Unfortunately, these inflammasome activating molecules cannot easily be chemically altered to investigate cellular regulation of the individual processes leading to inflammasome activation. There are two advantages to structurally driven probing of the inflammasome pathway, improved vaccine adjuvants and safer biomaterials. Currently, with a large number of vaccine adjuvants like

Received: April 10, 2018
Published: July 2, 2018

DOI: 10.1021/acscentsci.8b00218
ACS Cent. Sci. 2018, 4, 982−995

alum,[10] QS-21,[11] mmCT, dmLT,[12] etc. having been found to activate NLRP3 inflammasome, it can be envisioned that controlled inflammasome activation might assist in rational chemical design of vaccine adjuvants. Additionally, as many gene-delivery systems rupture endolysosomes, outlining criteria for inflammasome activation might help develop safer biomaterials. We envisioned elucidating a minimal structural and functional requirement for NLRP3 activation that would assist in engineering biomaterials that can activate NLRP3. Using a chemically controlled system would provide clear criteria for activation and design of immune potentiators. In seeking a method to control biological activity by a minimal change in chemical structure, we sought insight from the field of gene delivery. There, molecules have been intentionally designed to modulate individual biological processes in a controlled fashion, most notably, endolysosomal rupture.[13,14] In the present study we employ two polymers of similar molecular weight, chemical structure, and molecular architecture. Their only difference is in their capability to cause lysosomal rupture. One efficiently ruptures lysosomes (LR+) while the other is inefficient (LR−). The two compounds vary only in one parameter—the ratio of amino-acid-based dendrons to tetraethylene glycol (Figure 1 schematic diagram and Supporting Information for additional details). Since the structures of the polymers are otherwise analogous, we used these two polymers to design experiments that examined lysosomal rupture while controlling other factors involved in inflammasome activation. Our results demonstrate that the ability of these polymers to rupture the lysosome resulted in controlled activation of the inflammasome and subsequent IL-1β secretion by stimulated human THP-1 monocytes and murine bone-marrow-derived dendritic cells (BMDCs). These results suggested that lysosomal rupture is a critical regulator of inflammasome activation by the polymers since polymers with weak lysosomal rupture capabilities make weak inflammasome activators. Based on this understanding and the chemical control over inflammasome activation, we designed a minimal activation system which ruptures lysosomes, but requires only a short peptide coupled to an ethylene glycol sequence—demonstrating single amino acid precision in designing inflammasome activators.

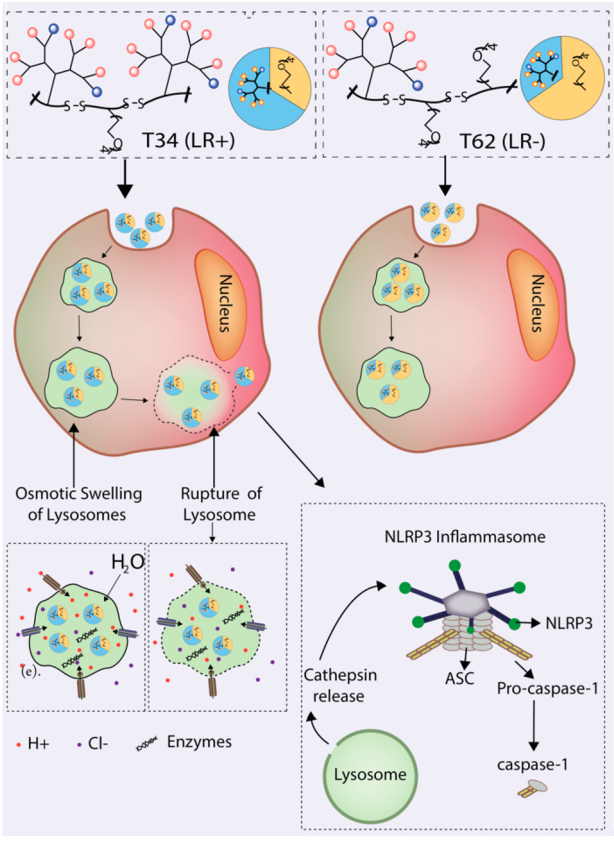

Figure 1. Structure of T34 (LR+) and T62 (LR−) (red, histidine; blue, tryptophan) and proposed mode of action. Pie-chart represents mole fraction of dendron and tetraethylene glycol.

RESULTS

A growing body of literature suggests that polymers with different molecular weights may activate inflammasomes due primarily to lysosomal rupture.[15] However, significant differences in structure, molecular weight, and molecular heterogeneity in these bioactive systems beg the question if other biological processes are at play.[16−18] To address these questions, we employed dendritic polymers of similar molecular weights that have a controlled arrangement of chemical moieties derived from a common scaffold, to use as a lysosomal rupture system.[19,20] Each of the dendritic polymers has multiple lysine-based dendrons (third generation) attached to a L-lysine-dicysteine backbone. The dendritic lysines are peripherally capped by histidine and tryptophan in a 3:1 molar ratio. The polymer backbones are also cofunctionalized by a certain percentage of tetraethylene glycol (TEG) chains to control spacing between adjacent dendrons. Previously, the polymers were denoted T34 and T62 based on the percentage of TEG in their structure.[19,20] Here, we denote them LR+ and LR−, respectively, based on their activity (Figure 1 schematic diagram; Figures S1 and S2, Supporting Information, for full chemical structure and characterization; Figure S3, Supporting Information, dynamic light scattering (DLS) characterization). Thus, LR+ and LR− have identical dendrons but differ only in the ratio between the dendrons and the TEG moieties.

Each polymer enters cells by endocytosis.[19,20] During endosomal acidification, the histidine residues become protonated, modifying the osmolarity of the intracellular compartment and resulting in rupture of the endolysosomes. The tryptophan residues assist cellular uptake and lysis of lysosomal membranes resulting in direct entry of the polymers into the cytosol.[19−21] Even though both polymers have identical components, LR+, with a greater number of dendrons and more sites for protonation, induces a greater change in osmolarity and more strongly ruptures lysosomes.

Select Polymers Induce NLRP3 Inflammasome Activation in THP-1 Cells. We incubated lipopolysaccharide-primed (LPS-primed) THP-1 cells either with LR+, LR−, or PBS for 0.5, 2, or 4 h along with DQ Green BSA—a fluorescent indicator of lysosomal proteolysis. BSA having an isoelectric point of around 5 is negatively charged at pH 7.4 and forms soluble complexes with the polymers (Figure S3, Supporting Information, for DLS characterization) resulting in cotrafficking across the cell membrane into endosomes. As observed from DLS data, the sizes of the complexes with LR+ and LR− at pH 7.4 and pH 5 were similar. The cells were also stained with propidium iodide to differentiate dead cells from live cells. By confocal microscopy, it was observed that the cells treated with either of the polymers had higher rates of DQ Green BSA uptake compared to PBS controls (Figure 2a).

DOI: 10.1021/acscentsci.8b00218
ACS Cent. Sci. 2018, 4, 982−995

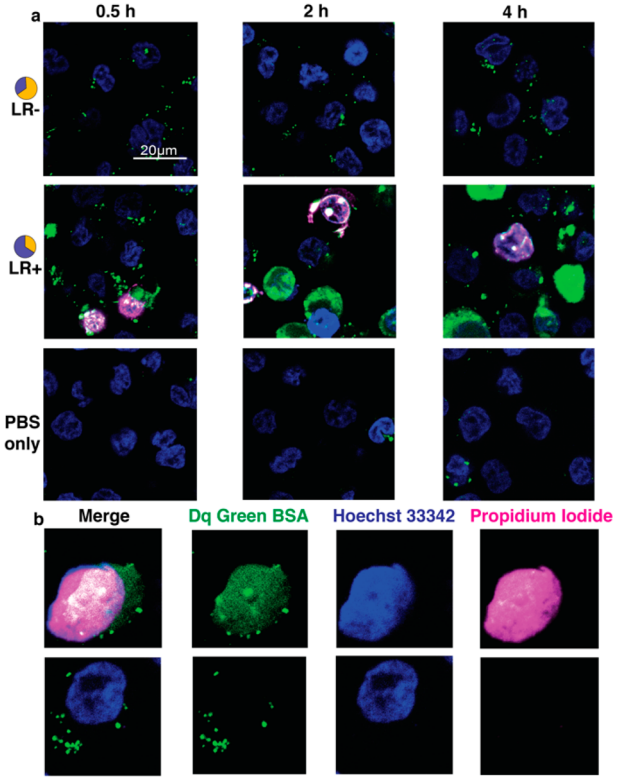

Figure 2. LPS-primed THP-1 cells treated with LR−, LR+ (0.04 mg/mL), or PBS along with DQ Green BSA, propidium iodide, and Hoechst 33342. (a) Representative cell images at 0.5, 2, and 4 h. (b) Typical dead (top) and a normal healthy live (bottom) cell.

While cells treated with LR− or PBS had DQ Green BSA localized in distinct punctate endolysosomes, cells treated with LR+ had numerous swollen lysosomes in more than 40% of the cells within 0.5 h as analyzed by confocal microscopy. While normal lysosomes measured around 0.25 μm^2, swollen lysosomes were mostly observed to vary anywhere between 1 μm^2 to upward of 9 μm^2 as observed by microscopy. (Figure S4, Supporting Information). DQ BSA diffused into the cytosol beginning at the 0.5 h time point for the LR+-treated cells. We concluded that this diffusion of DQ Green BSA throughout the cytosol was the result of lysosomal rupture by LR+. Even though we observed some swollen lysosomes in cells treated with LR− after 2 h, very few cells had DQ Green BSA present in the cytosol. We further observed that a significant fraction of the cells treated with LR+ were stained with propidium iodide starting at the 0.5 h time point while there were no observable dead cells in the LR− and PBS samples. In addition, for the LR+-treated cells we found progressively higher amounts of swollen endolysosomes at 2 and 4 h. On analysis of dead and live cells in the LR+ population, we observed that, for dead cells, the DQ Green BSA was significantly delocalized throughout the cytosol, whereas for live cells it was mostly confined in small, distinct endolysosomal compartments (Figure 2b).

We further used another fluorescent reagent fluorescein isothiocyanate-dextran (FITC-dextran) to track cellular uptake of these polymers. It was observed that incubation of LPS-primed THP-1 cells with either LR+ or LR− significantly enhanced uptake compared to controls as observed by flow cytometry (Figure S5, Supporting Information) or confocal microscopy (Figure S6, Supporting Information). Confocal microscopy indicated diffusion of FITC-dextran in LR+-treated cells while FITC-dextran in LR−-treated cells appeared mostly small and punctate. Further, significant cell death was observed in LR+-treated cells as indicated by propidium iodide staining while propidium iodide staining in LR−-treated cells was similar to control levels.

Hence, we concluded that LR+ was a more potent lysosome rupturing polymer compared to LR−, resulting in cell death in LPS-primed THP-1 cells.

To test the role of lysosomal rupture and the nature of cell death caused by the polymers, we incubated THP-1 cells (3.6×10^5) with LR+ or LR− (8 μg), or PBS for 4 h after priming with ultrapure LPS. It was observed that bioactive IL-1β was secreted by the THP-1 cells, as measured by HEK-Blue IL-1β reporter cells using Quanti-Blue reagent (see the Methods section for details). LR+-treated cells secreted high amounts of IL-1β, whereas IL-1β secreted by cells incubated with LR− was comparable to that of the PBS control (Figure 3a). To confirm that the polymers were operating through a classical NLRP3 inflammasome pathway, we incubated LR+ and LR− with ASC knock-down (THP-1shasc) and caspase-1 knock-down (THP-1shcasp1) cells (Figure 3b; ASC, apoptosis-associated speck-like protein containing a caspase recruitment domain). In each case, the knock-down THP-1 cells reduced the IL-1β secretion to background levels while THP-1 cells transfected with a scrambled shRNA (THP-1shscr) showed similar IL-1β activity as untreated THP-1 cells. Further, treatment of THP-1 cells with the NLRP3 inhibitor isoliquiritigenin[22] reduced IL-1β secretion to levels akin to negative controls (Figure 3a).

To test if the activation was mediated solely by NLRP3, we used MCC950,[23] an inhibitor that selectively inhibits NLRP3 and not AIM2, NLRP1, and NLRP4. Inhibition with MCC950 reduced the IL-1β secretion to background levels. We further validated the dependence on NLRP3 and the biological relevance in primary cells, by testing LR± and IL-1β secretion with wild type (WT) and NLRP3$^{-/-}$ BMDCs (Figure 3d). It was observed that LR+ induced a 13-fold higher secretion of IL-1β compared to LR− in WT BMDCs as measured by IL-1β ELISA. Further, the same experiment conducted on NLRP3$^{-/-}$ BMDCs reduced the IL-1β secretion to background levels. This experiment led us to conclude that IL-1β is generated due to activation of the NLRP3 inflammasome by the polymers, and LR+ is a strong inflammasome inducer relative to LR−.

We further compared inflammasome activation by the polymers by monitoring the inflammasome adaptor protein ASC in THP-1 cells. Upon inflammasome activation, ASC forms a prion-like assembly into a filamentous high-molecular-weight complex referred to as the pyroptosome.[24−26] After LPS-primed THP-1 cells were treated with LR+ or LR−, cells were fixed at different time intervals and stained for ASC (see the Methods section for details). We observed that, from a cell culture treated with LR+, only about ∼10% of cells showed pyroptosome formation and inflammasome activation, whereas cells treated with LR− did not induce any observable pyroptosome formation (Figure 3c). This result is in contrast to other inflammasome activators where >75% of cells can appear activated. Intrigued by the lower percentage of active cells contrasted with the high response, we proceeded to examine whether endolysosomal rupture was the element that primarily controlled activation of ASC and pyroptosis and enabled inflammasome activation by the polymers.

Since NLRP3 inflammasome activation leads to the formation of active caspase-1,[2] we compared the caspase-1

DOI: 10.1021/acscentsci.8b00218
ACS Cent. Sci. 2018, 4, 982−995

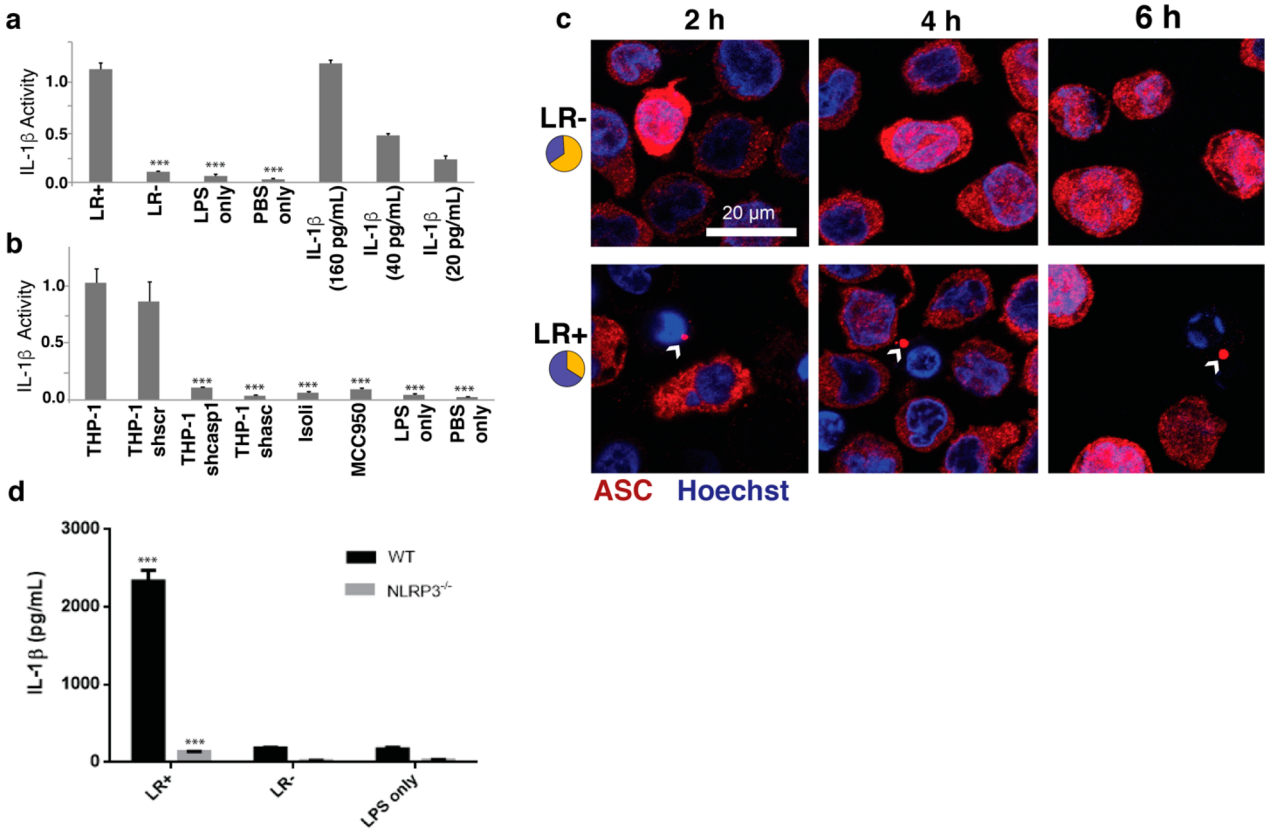

Figure 3. Induction of NLRP3 inflammasome activation by LR− and LR+ (0.04 mg/mL). (a) IL-1β production in LPS-primed THP-1 cells on treatment with LR− and LR+ for 4 h; response generated by recombinant IL-1β is used as a reference (***$p < 0.001$, statistical analysis conducted against LR+ sample). (b) IL-1β induced by LR+ on various knock-down cells on treatment with NLRP3 inhibitors isoliquiritigenin (isoli) and MCC 950 (***$p < 0.001$, statistical analysis conducted against THP-1 sample). (c) Fixed THP-1 cells stained with anti-ASC antibody to study pyroptosome formation following treatment with LR− or LR+ for 2, 4, or 6 h following transcriptional priming with LPS for 3 h. Pyroptosome-forming cells indicated with arrow. (d) IL-1β induced by LR+ on WT and NLRP3$^{-/-}$ BMDCs measured by IL-1β ELISA (***$p < 0.001$, statistical analysis conducted against respective LR− sample).

activity induced by each polymer. Following priming with LPS, THP-1 cells were treated for 2, 4, or 6 h with either LR+, LR−, or PBS. The cells were then washed and incubated with FAM-YVAD-FMK, a cell-permeable, irreversible binder of caspase-1. The cells were also stained with propidium iodide. We analyzed 10 000 events for each condition on an Amnis ImageStream flow microscope. We observed two distinct populations of cells for each sample as shown in Figure 4. Representative cells from each population are also shown (Figure 4d,e). One of the populations shows no fluorescence from FAM-YVAD-FMK or propidium iodide, indicating they are normal, healthy cells while the other population fluoresced green from the FAM-YVAD-FMK, indicating caspase-1 activity. This population exhibiting caspase-1 activity was also stained with propidium iodide. This indicated the cell death observed due to incubation with the polymers was the result of inflammasome activation and pyroptosis. It was observed that while LR+ induced inflammasome activation in a significant number of cells, inflammasome activation by LR− was not substantially different from the control samples. We further observed that the maximum response from the polymers was obtained after about 4 h. From this we concluded that the small difference in the arrangement of chemical structures on a common polymer scaffold leads to cell death due to pyroptosis and induces significant differences in inflammasome activity.

Phagocytosis Followed by Endolysosomal Rupture Is Necessary for Inflammasome Activation by Polymers. LR+ appeared to activate the inflammasome in only a subset of cells, and that subset exhibited lysosomal rupture as evident from the DQ Green BSA studies (Figure 2). To directly observe the polymers, we conjugated Alexa Fluor 488 to them (see the Supporting Information for synthesis). Following priming of the THP-1 cells with LPS, they were incubated with the labeled polymers LR+/Fl or LR−/Fl. We further stained the cells with Lysoview 633, a pH-sensitive fluorogenic dye that stains acidic organelles, thereby permitting visualization of endolysosomal compartments. The cells were also stained with Hoechst 33342 and propidium iodide. Following incubation for 0.5, 2, and 4 h, the cells were washed and imaged. Figure 5a,b shows representative images of cells incubated with LR +/Fl or LR−/Fl at different time intervals. Based on the propidium iodide stain, we observed approximately 10% pyroptosing cells in the sample treated with LR+/Fl while we found cells treated with LR−/Fl were pyroptosing at very low levels similar to PBS only controls. Even though we observed diffused lysosomes in a fraction of cells treated with LR+/Fl or LR−/Fl, we observed the LR−/Fl mostly localized in endolysosomes while a percentage of cells treated with LR +/Fl showed the polymer outside of the lysosome. On a careful analysis of pyroptosing and normal cells in the LR+/Fl sample, it was observed that all pyroptosing cells had high amounts of

DOI: 10.1021/acscentsci.8b00218
ACS Cent. Sci. 2018, 4, 982−995

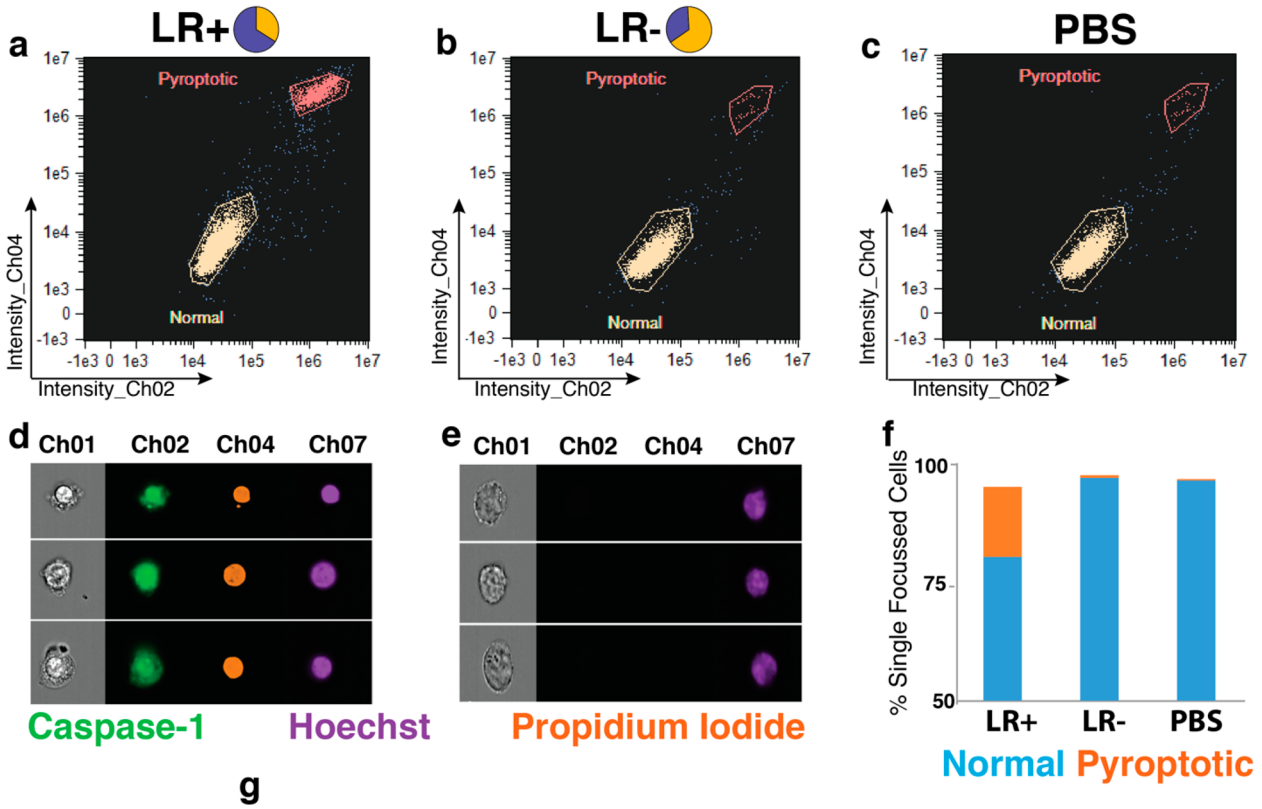

g

Time	Cell percentage	LR+	LR-	LPS only
2 h	% pyroptotic	14.94	0.46	0.25
	% normal	81.01	97.98	97.93
4 h	% pyroptotic	21.17	1.21	1.06
	% normal	67.32	91.56	92.09
6 h	% pyroptotic	22.53	1.41	2.23
	% normal	71.93	96.0	93.27

Figure 4. Inflammasome activation by LR+, LR− (0.04 mg/mL), and PBS measured on an Amnis ImageStream instrument by staining cells with FAM-YVAD-FMK, propidium iodide, and Hoechst 33342. For each sample, 10 000 events were recorded out of which only single focused cells were used for further analyses. The channels are brightfield (Channel 01), caspase-1 (Channel 02), propidium iodide (Channel 04), and Hoechst 33342 (Channel 07). Flow cytometric analyses are presented for samples transcriptionally primed with LPS for 3 h followed by incubation for 2 h with LR+ (a), LR− (b), and PBS (c). Two distinct populations of cells were observed. Typical pyroptotic cells displayed both caspase-1 and propidium iodide activity (d) while normal cells were not stained by FAM-YVAD-FMK or propidium iodide (e). (f) Percentage of normal and pyroptotic cells in each sample at 2 h. (g) Variation in the percentage of normal and pyroptotic cells in each sample over time.

LR+/Fl in the cytosol, a difference from live cells which had the polymers localized in endolysosomes (Figure 5c). These studies validated that the polymers gather in the endolysosomes and support the hypothesis that it is the rupture of the lysosomes containing LR+ that led to the result observed in our DQ Green BSA studies earlier (Figure 2). We further investigated the role of phagocytosis and lysosomal rupture in inflammasome activation using phagocytosis and lysosomal acidification inhibitors. Among a number of inhibitors tested, we observed that filipin-III, monensin, and ammonium chloride significantly reduced IL-1β secretion by THP-1 cells following incubation with LR+ (Figure 6). We probed these observations using flow cytometry (Figure 6a−c) and confocal microscopy (Figure 6d−g). Alexa-Fluor-488-labeled LR+ were used to visualize the polymers, whereas Hoechst 33342 and Lysoview 633 were used to stain the nuclei and lysosomes of

DOI: 10.1021/acscentsci.8b00218
ACS Cent. Sci. 2018, 4, 982−995

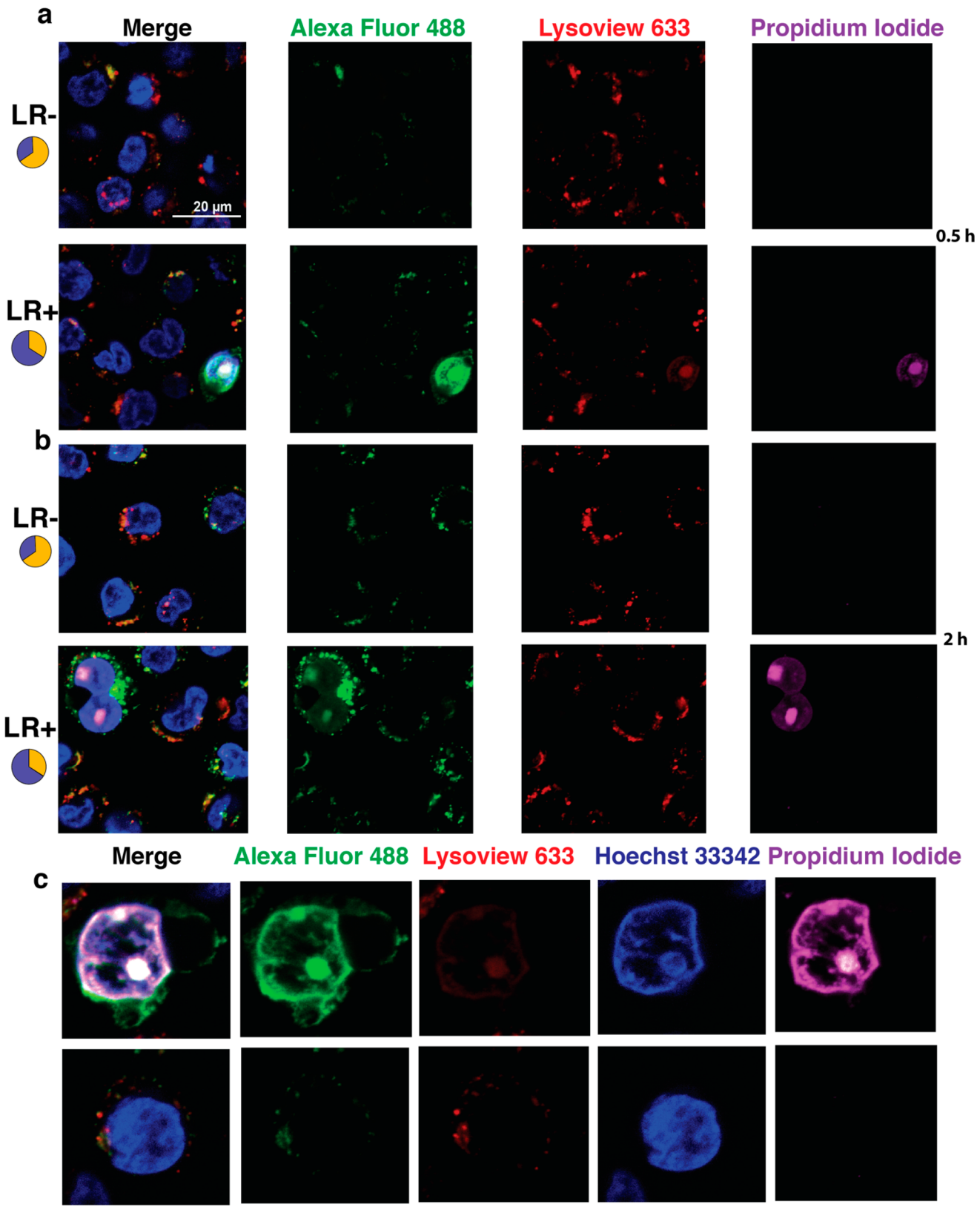

Figure 5. THP-1 cells primed with LPS for 3 h followed by treatment with AF-488-labeled polymers (0.04 mg/mL) along with LV 633, Hoechst 33342, and propidium iodide and imaged at 0.5 h (a) and 2 h (b). (c) Representative pyroptotic cell (top) and a live cell (bottom).

the cells, respectively. To study the rate of phagocytosis we monitored changes in the rate of Alexa-Fluor-labeled LR+ uptake, and we examined changes in lysosomal acidity based on changes in the intensity and number of Lysoview-633-stained organelles. It was observed that while phagocytosis was inhibited by filipin-III, it did not have any observable effect on lysosomal acidification. However, monensin and ammonium chloride acted to both inhibit phagocytosis and to reduce

DOI: 10.1021/acscentsci.8b00218
ACS Cent. Sci. 2018, 4, 982−995

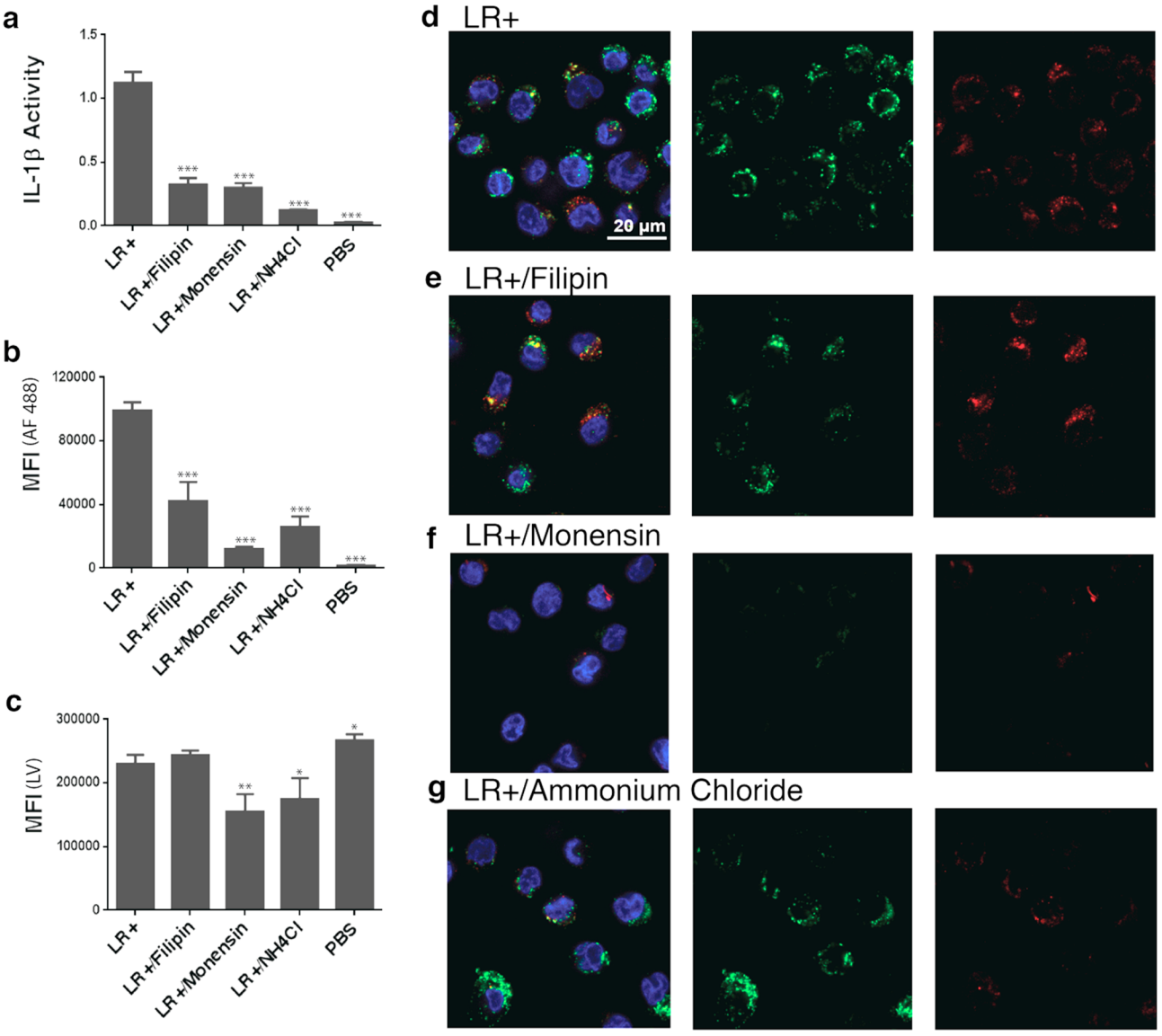

Figure 6. Role of phagocytosis and lysosomal rupture. THP-1 cells treated with LR+ or LR+/Fl (0.04 mg/mL) with or without inhibitors for 4 h following priming with LPS for 3 h. (a) IL-1β activity with THP-1 cells treated with LR+ with and without inhibitors. (b) Median fluorescence intensity of LR+/Fl-treated cells measured by flow cytometry with and without inhibitors indicating the rate of phagocytosis. (c) Median fluorescence intensity of Lysoview 633 in LR+-treated cells measured by flow cytometry with and without inhibitors indicating lysosomal acidity (***$p < 0.001$, **$p < 0.01$, *$p < 0.05$; statistical analysis conducted against LR+ sample). Confocal microscopy image of THP-1 cells treated with LR+/Fl without inhibitors (d) or with filipin-III (e), monensin (f), or ammonium chloride (g).

lysosomal acidity. This indicates that the polymers need to be internalized for subsequent inflammasome activation. Hence, it can be concluded for our dendronized polymers that phagocytosis, acidification of endolysosomes, and subsequent lysosomal rupture play a significant role in the regulation of NLRP3 inflammasome activity.

Among lysosomal enzymes, cathepsins, particularly cathepsin B, are proposed to be involved in inflammasome activation.[8,27,28] NLRP3 binds to cathepsin B as demonstrated by coprecipitation using either an anti-NLRP3 or an anti-cathepsin B antibody.[9] Cathepsin B activates stress responsive mitogen-activated protein kinases (MAPK) and specifically the TAK1-JNK pathway[29] have been implicated to be necessary for NLRP3 inflammasome activation. Hence, we studied the effect of cathepsin B, kinases, and TAK1-JNK on inflammasome activation by the polymers on THP-1 cells. It was observed that the addition of cathepsin B inhibitor CA-074-Me or cysteine protease inhibitor E 64d reduced IL-1β secretion by about 70% upon addition of LR+ (Figure 7a). Further addition of TAK1 inhibitors like (5Z)-7-Oxozeaenol[29] or Takinib[30] significantly reduced IL-1β secretion to the same level as inhibition by cathepsin B, implying that the pathway was mediated primarily through cathepsin B activation of MAPK and TAK1-JNK as has been seen for other inflammasome activators.[29]

We further used the cathepsin B substrate reagent MR-$(RR)_2$—a fluorescent probe—to detect cathepsin B activity in live cells treated with the polymers. THP-1 cells were incubated with LR+ and LR− for different time intervals (2, 4, 6 h) followed by addition of MR-$(RR)_2$. Upon imaging, we observed that cells incubated with LR+ showed significant red fluorescence, indicating cathepsin B activity whereas that activity was much lower in cells incubated with LR− (Figure 7b).

DOI: 10.1021/acscentsci.8b00218
ACS Cent. Sci. 2018, 4, 982−995

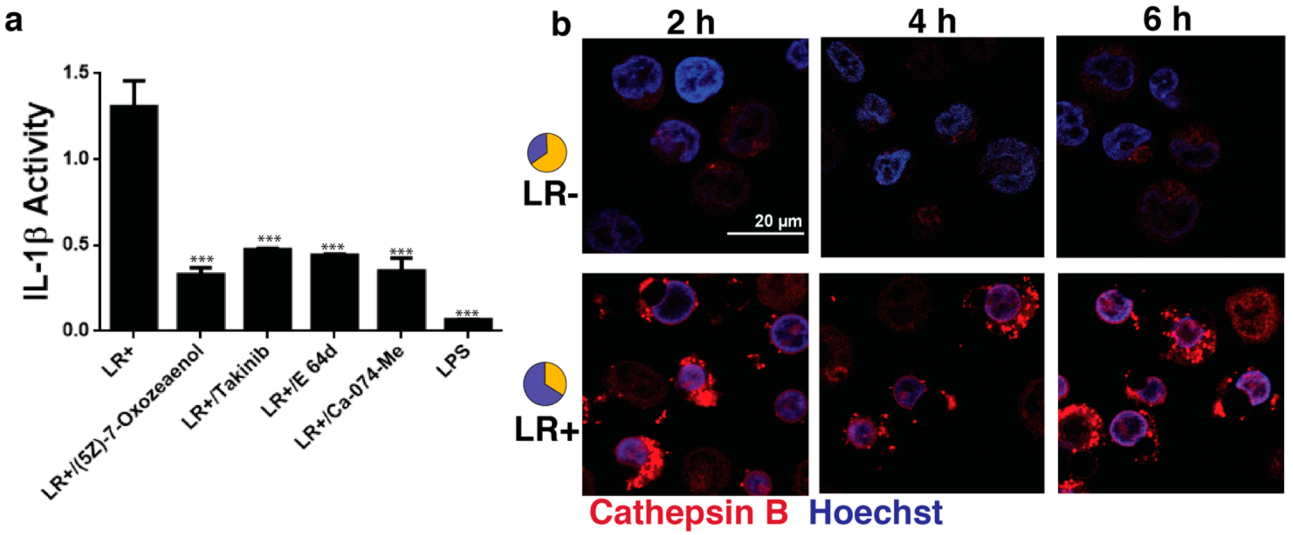

Figure 7. Role of lysosomal enzymes. (a) IL-1β activity in THP-1 cells stimulated with LR+ (0.04 mg/mL) in presence or absence of TAK1 inhibitors (5Z)-7-Oxozeaenol and Takinib; protease inhibitor E 64d and cathepsin-B inhibitor Ca-074-Me for 4 h following treatment with LPS for 3 h (***$p < 0.001$, statistical analysis conducted against LR+ sample). (b) Cathepsin B activity of THP-1 cells treated with LR− (top) or LR+ (bottom) along with cathepsin B substrate reagent MR-(RR)2.

This suggested a role of cathepsin B and a kinase-mediated pathway following lysosomal rupture in inflammasome activation by the polymers.

Role of ROS Production. Since mitochondrial ROS production has been implicated in NLRP3 inflammasome activation,[31] we looked for ROS production in THP-1 cells following treatment with the polymers using Cell Rox Green. It was observed that even the addition of higher amounts of LR+ (20 μg) did not lead to any significant ROS production compared to the LPS only and PBS only controls (Figure S7, Supporting Information). It can be concluded that ROS production does not play a significant role in the induction of inflammasome activation by the polymers.

Role of Potassium Efflux. Since cytosolic potassium efflux triggers NLRP3 inflammasome activation,[6] we investigated the role of potassium efflux in inflammasome activation by the polymers. It was observed that secretion of IL-1β was reduced significantly when THP-1 cells were treated with 25 mM or higher amounts of extracellular KCl before the addition of the polymers (data not shown). Given that, we decided to investigate the sequence of events leading up to potassium efflux and consequent inflammasome activation. Following priming with LPS, THP-1 cells were stained with Hoechst 33342, Lysoview 633, propidium iodide, and Asante Potassium Green-4 (APG-4), a fluorescent potassium indicator that binds cytosolic potassium. Following this, LR+ was added to the cells, and images were obtained at regular intervals for 30 min (Figure 8e). It was observed that the Lysoview-633-stained organelles were reduced over time indicating rupture of lysosomes. The cells losing the Lysoview 633 stain were simultaneously observed to have a decrease in the APG-4 intensity indicating loss of potassium due to efflux. The events occurred almost concurrently, within a 0−5 min interval from one another, indicating a likely concerted mode of action. It was further observed that cells losing Lysoview 633 and APG-4 were subsequently stained by propidium iodide.

To further confirm these observations, we performed experiments using an ImageStream instrument. After THP-1 cells were primed with LPS for 3 h, they were incubated with LR+ polymers and stained with Lysoview 633, APG-4, Hoechst 33342, and propidium iodide. We observed three distinct populations of cells (Figure 8a). Cells in the live population were stained intensely with both Lysoview 633 and APG-4 and were not stained by propidium iodide (Figure 8b). A pyroptosing population of cells was also observed that stained faintly with Lysoview 633 indicating extensive lysosomal rupture. These same cells had low levels of APG-4 stain indicating that potassium had effluxed out of these cells. The same population of cells also stained intensely with propidium iodide (Figure 8d). We further observed a population that stained with Lysoview 633 and APG-4 stain at a lower intensity than live cells. These cells also had weaker propidium iodide staining than the pyroptosing population (Figure 8c). We termed this population of cells as effluxing. We measured the median intensity of APG-4 in each of these populations. The fluorescence intensity in the live population was $481 \pm 219.5 \times 10^3$ a.u., whereas the fluorescence intensity in the pyroptosing and effluxing populations were found to be $118.4 \pm 76.3 \times 10^3$ a.u. and $282.4 \pm 153.4 \times 10^3$ a.u., respectively (a.u., arbitrary units).

Thus, it can be noted that the polymers induce lysosomal rupture which leads to concurrent potassium efflux, and these processes were observed to occur within short intervals of one another. Efflux of potassium from the cells leads to subsequent cell death as observed by the propidium iodide stain.

Immunomodulation of Inflammasome Activity by Variations in Chemical Structure. Polymer LR+ (T34) ruptures lysosomes upon acidification, resulting in clear and distinct activation of the inflammasome. We noted that only cells which contained a high degree of active LR+ resulted in inflammasome activation (Figure 5). In contrast, LR− (T62) did not result in detectable lysosomal rupture or substantial inflammasome activation. With this structural and functional understanding, we hypothesized that, by controlling the degree of endolysosomal rupture or, phrased another way, the probability of lysosomes rupturing, we might control the amount of IL-1β secretion by a pseudostatistical process of limiting the number of cells with active inflammasomes. To

DOI: 10.1021/acscentsci.8b00218
ACS Cent. Sci. 2018, 4, 982−995

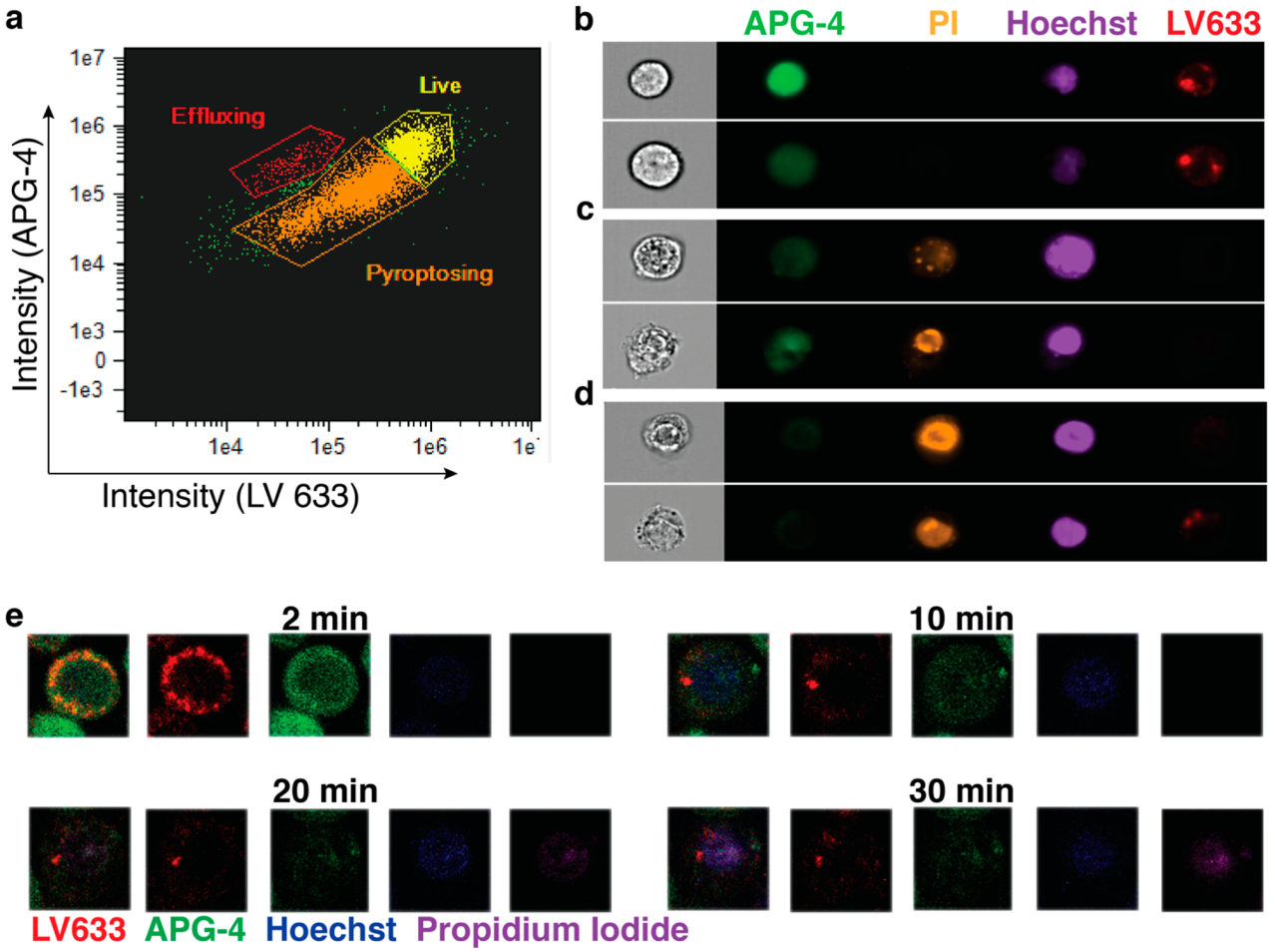

Figure 8. Study of lysosomal rupture and potassium efflux. THP-1 cells were primed with LPS followed by treatment with LR+ (0.1 mg/mL) for 30 min and stained with APG-4, propidium iodide, Hoechst 33342, and LV 633. (a) Flow cytometry analysis with the plot of the intensity of APG-4 vs LV 633. Three distinct populations of cells were observed. (b) Typical live cells with intense APG-4 stain and intact or partially ruptured lysosomes. (c) Typical cells with ruptured lysosomes and effluxing potassium starting to stain with propidium iodide. (d) Typical pyroptotic cells with fully or partially ruptured lysosomes and with low levels of potassium due to efflux. These cells also stain with propidium iodide. (e) THP-1 cells were treated with LR+ along with APG-4, LV 633, Hoechst 33342, and PI and monitored over 30 min. A representative pyroptosing cell is shown at different time intervals.

test this hypothesis, we synthesized few analogous polymers using the same linear L-lysine-dicysteine scaffold. The polymers varied either in the amount of TEG relative to the dendrons or in the ratio of histidines to tryptophans in the dendrons (see ref 20 for synthesis). The polymers are named by their percentage of TEG denoted by the letter T followed by the ratio of histidines to tryptophans in the dendrons (Figure 9a,b). It was observed that THP-1 cells (3.6×10^5) incubated with the library of chemically analogous polymers (20 μg) secreted significantly different amounts of IL-1β. Increasing the TEG content from 32% to 42% to 62% in the dendritic polymers significantly decreased IL-1β secretion by the cells (Figure 9a). T42, being intermediate between T34 and T62, secreted greater amounts of IL-1β compared to T62 but significantly lower than T34. This agrees well with the data that T34 induces a higher rate of endolysosomal rupture compared to T42 or T62, inducing higher IL-1β secretion and suggesting that controlling the degree of lysosomal rupture can control the degree of activation of the inflammasome. Further, as seen in Figure 9a, it was observed decreasing the TEG content from 34% to 0% reduced IL-1β secretion. It could be that some amount of TEG spacing between bulky dendrons relieves unfavored intramolecular interactions between adjacent dendrons, leading to more efficient endolysosomal rupture. Further, differences in the composition of the dendrons were observed to induce changes in the inflammasome activity (Figure 9b). It was seen that changes in the ratio of histidines and tryptophans in the T0 polymers induced different amounts of IL-1β secretion. A certain ratio of histidine and tryptophans was found to be necessary for optimal activity of the polymers. A ratio of 2:1 histidines to tryptophans in the polymers induced the highest amount of IL-1β secretion by the polymers. However, ratios of 1:3 or 3:1 gave reduced activity, possibly due to a less than optimal number of histidines and tryptophans, respectively, necessary for efficient proton sponging or membrane lysis. Both 1:2 and 1:1 showed still lower activity possibly because they did not contain optimal ratio of histidines to tryptophans necessary for proton sponging and membrane lysis. The solubility of these compounds was further assessed using dynamic light scattering (DLS) to discount other physical parameters (see the Supporting Information, Figure S8). The compounds with 50 or higher percentage of histidines were found to be highly water-soluble. T0/1:2 formed a mildly turbid solution at pH

DOI: 10.1021/acscentsci.8b00218
ACS Cent. Sci. 2018, 4, 982−995

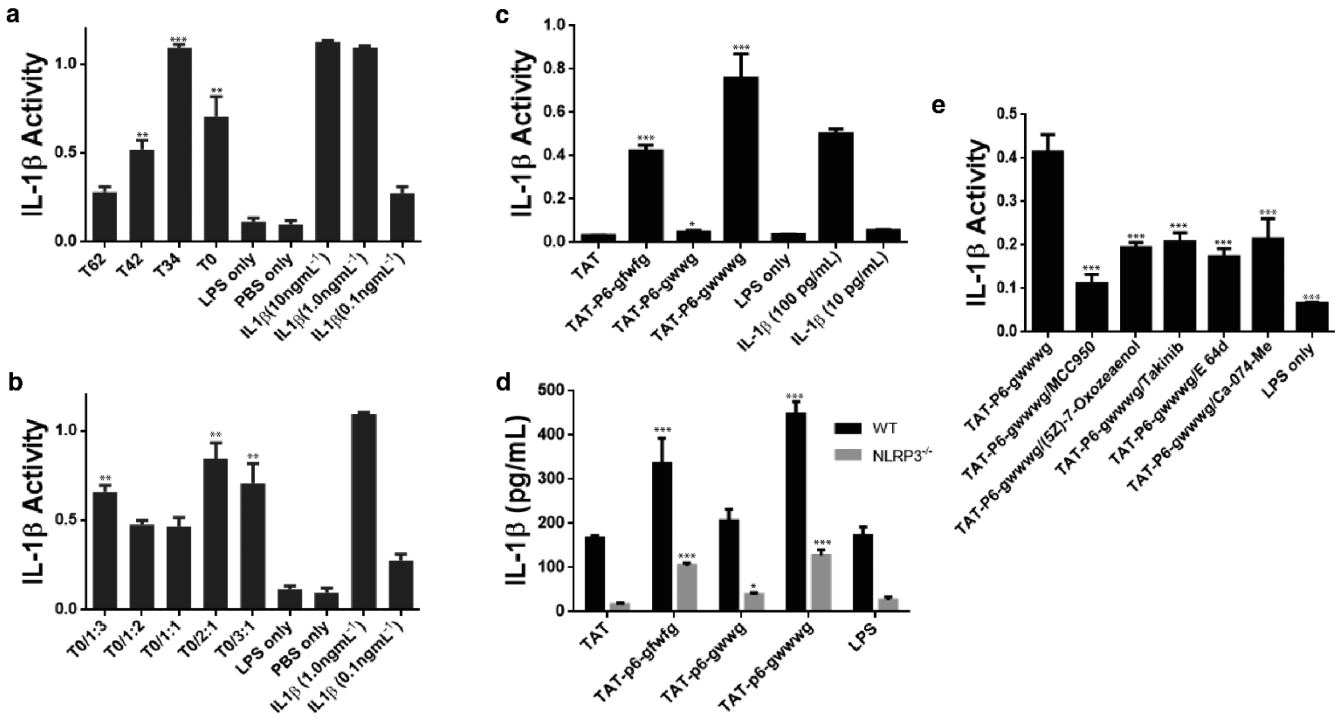

Figure 9. Immunomodulation of NLRP3 inflammasome. (a, b) IL-1β activity in THP-1 cells stimulated with a library of polymers (0.1 mg/mL). The polymers are assigned by the percentage of TEG denoted by T and the ratio of histidine to tryptophan in the dendrons: (a) comparison between polymers with varying amounts of TEG; (b) comparison between polymers with different ratio of histidines to tryptophans (**$p < 0.01$, ***$p < 0.001$, statistical analysis conducted against T62 sample in part a and T0/1:1 sample in part b). (c, d) IL-1β activity in cells stimulated with a library of TAT peptides (20 μM): (c) IL-1β activity in THP-1 cells treated with TAT peptides for 4 h following priming with LPS for 3 h (*$p <$ 0.05, ***$p < 0.001$, statistical analysis conducted against TAT sample). Response generated by human recombinant IL-1β standards are used as a reference in parts a–c. (d) IL-1β activity by WT and NLRP3$^{-/-}$ BMDCs treated with TAT peptides for 4 h following priming with LPS for 3 h (*p < 0.05, ***$p < 0.001$, statistical analysis conducted against respective TAT sample). (e) IL-1β activity in THP-1 cells treated with TAT-P6-gwwwg with and without inhibitors for 4 h following transcriptional priming with LPS for 3 h (***$p < 0.001$, statistical analysis conducted against TAT-P6-gwwwg sample).

7.4 and had a mean hydrodynamic radius of 100 nm, possibly owing to mild aggregation. T0/1:3 formed a cloudy suspension without any obvious precipitation. However, both these polymers formed clear solution at pH 5 indicating they were highly soluble at endo-/lysosomal pH. At this pH, DLS data indicated a hydrodynamic radius around 50 nm, similar to the other polymers studied indicating no obvious aggregation. However, a contributing factor due to lower cellular uptake cannot be ruled out. Thus, this suggests that controlling the endolysosomal rupture by variations in chemical structure can limit the amount of inflammasome activation.

As seen in Figure 9a, it was further observed that 20 μg of T34 induced about 1 ng/mL of IL-1β compared to 0.16 ng/mL using 8 μg of T34 (Figure 3a). Further, T62 induced significant amounts of IL-1β secretion at 20 μg compared to PBS controls, while it did not induce any IL-1β secretion at 8 μg. ImageStream analysis indicated that T34 induced pyroptosis in about 15% of cells using 8 μg within 2 h while the percentage rose to about 70% when 20 μg was used (data not shown). This suggests the possibility of a cellular machinery to control inflammasome activation by threshold effect of endolysosomal rupture in cells indicating a certain amount of endolysosomal rupture is possibly tolerated beyond which there is rapid inflammasome activation.

To help test the core principles of the activation and the key elements of the polymers, we tried to design simple, druglike peptide-based inflammasome activators using the principles of the polymer system. We examined a cell penetrating TAT peptide (HIV-1 TAT protein (47–57); YGRKKRRQRRR) modified with the addition of hydrophobic endosomal escape domains developed by Lonn et al.[32] (see the Methods section for experimental details, and the Supporting Information for characterization). It was observed that addition of the hydrophobic domains to TAT significantly induced IL-1β secretion when added at a 20 μM concentration to LPS-primed THP-1 cells (2×10^6 cells/mL) (Figure 9c) or WT BMDCs (1×10^6 cells/mL) (Figure 9d). In contrast, the unmodified TAT peptide at 20 μM concentration did not induce significant IL-1β secretion compared to LPS only controls. To determine the degree of control for which the hydrophobic and TAT peptides balanced the inflammasome activity, we varied the hydrophobic domains GFWFG, GWWG, and GWWWG attached to the TAT peptide via a hexaethylene glycol (referred to as P6). All the modified peptides demonstrated statistically significant IL-1β activity compared to TAT in THP-1 cells while the GFWFG and GWWWG modified peptides demonstrated statistically significant IL-1β activity in WT BMDCs. The IL-1β activity was significantly reduced in THP-1 cells when selective NLRP3 inhibitor MCC950 (Figure 9e) was added to the cells. Further, the IL-1β activity was significantly attenuated in NLRP3$^{-/-}$ BMDCs indicating the IL-1β activity was primarily mediated via NLRP3 activation. Addition of inhibitors (5Z)-7-Oxozeaenol, Takinib, E 64d, and Ca-074-Me was observed to induce significant reduction in IL-1β activity in THP-1 cells indicating a kinase-mediated mode of action (Figure 9e). Further, it observed a difference of one

DOI: 10.1021/acscentsci.8b00218
ACS Cent. Sci. 2018, 4, 982–995

tryptophan (W) between the GWWG and the GWWWG modified peptides induced a difference of IL-1β activity greater than 10-fold in THP-1 cells and about 5-fold in BMDCs (baseline subtraction from LPS only sample).

Thus, we concluded that it is possible to rationally design immunomodulatory inflammasome activators based on a single controlled mode of activation of balancing hydrophobicity with membrane adhesion properties.

DISCUSSION

The NLRP3 inflammasome is activated by a diverse array of stimuli leading to multiple cellular events. Even though extensive studies have been performed on these stimuli and the role of each of these cellular events in inflammasome activation, the understanding of these processes is still incomplete due to the absence of proper chemical controls. Previous extensive studies of inflammasome activation have demonstrated lysosomal rupture,[8] ROS production,[27] membrane permeabilization,[6] etc. as agents for inflammasome activation. However, each these systems are highly chemically undefined, and most of these activators trigger multiple cellular events. As such, with just biological controls and in the absence of proper or practically any chemical controls these observations remain partially proven accepted facts. By designing a system allowing us to precisely control only one factor without conflating others, we demonstrated two systems where rupture from endolysosomes serves as a key controller and a minimal requirement for initiating inflammasome activation. Further, by single amino acid manipulation of the structure of our stimuli, we demonstrated that it is possible to partially predict and design the degree of inflammasome activity from a compound. This understanding may help to guide the design of immunomodulatory particles for therapeutic and prophylactic purposes where partial activation is desired. Further, this may lead to the development of dosable inflammasome activators as vaccine adjuvants. Currently, a large number of adjuvants have been demonstrated to activate NLRP3 inflammasome. However, most these compounds such as QS-21[11] are natural products[33] or compounds like mmCT, dmLT,[12] etc. that are derived from pathogens. However, in spite of the fact that some of these molecules are highly potent adjuvants, unfortunately a major drawback is that they are cumbersome to be chemically synthesized in large scales, and neither can they be easily tweaked to modulate their activities. On the contrary, rationally designed chemically synthesized activators can easily be chemically altered to obtain immunomodulation. Thus, a library of these compounds with varying immunological profiles can be synthesized with relative ease. Hence, such a design holds huge promise for the development of more efficacious and safer biomaterials. Based on this concept, we are working toward developing a bigger chemical toolbox to elicit predictable degrees of inflammasome activation.

METHODS

Safety Statement. No unexpected or unusually high safety hazards were encountered.

Reagents. All reagents and solvents were purchased from commercial suppliers (Sigma-Aldrich, Alfa Aesar, Fluka, TCI America). Ultrapure LPS, anti-IL-1β antibody, isoliquiritigenin, and MCC950 were purchased from Invivogen. All cell media, Hoechst 33342, DQ Green BSA, and Alexa Flour 488-NHS were bought from Thermo Fischer Scientific. Lysoview 633 was obtained from Biotium. APG-4 was purchased from TEFLabs, monensin from Tocris, and filipin-III from Sigma-Aldrich. Propidium iodide, FAM-YVAD-FMK kit (FAM FLICA Caspase-1), and cathepsin B MM-$(RR)_2$ kit (Magic Red cathepsin B) were bought from Immunochemistry Technologies. Ca-074-Me was obtained from Calbiochem. E 64d and (5Z)-7-Oxozeaenol were from Tocris. Takinib was from Medchemexpress. Rabbit polyclonal anti-TMS1 and donkey antirabbit IgG Alexa Fluor 647 antibodies were purchased from Abcam. All peptide synthesis reagents were purchased from Novabiochem. Fmoc-N-amido-dPEG$_6$-acid linker was purchased from Quanta Biodesign, and azidohexanoic acid was purchased from Click Chemistry Tools.

Cells. THP-1 cells were purchased from ATCC, and HEK Blue-IL-1β cells were from Invivogen. THP-1shasc, THP-1shscr, and THP-1shcasp1 cells were obtained as reported previously.[34] THP-1, THP-1shasc, THP-1shscr, and THP-1shcasp1 cells were used at a density of 2×10^6 cells/mL. These cells were cultured in RPMI 1640 growth media supplemented with penicillin (50 μg/mL) and streptomycin (50 μg/mL) along with 10% (v/v) FBS. HEK Blue IL-1β cells were used at a density of 5×10^5 cells/mL. The cells were cultured in DMEM media supplemented with glucose (4.5 g/L), L-glutamine (584 mg/L), penicillin (50 μg/mL), streptomycin (50 μg/mL), Normocin (100 μg/mL), Hygromycin-B Gold (200 μg/mL), and Zeocin (100 μg/mL). In place of FBS, 10% (v/v) heat-inactivated FBS was used for cell assays.

IL-1β Assay. THP-1 cells (3.6×10^5) were plated in 96-well plates at a density of 2×10^6 cells/mL in RPMI media supplemented with heat-inactivated FBS following which they were treated with ultrapure LPS (100 EU/mL). After incubation for 3 h the supernatant was removed, and the cells were supplemented with fresh media and treated with the polymers or TAT peptides for 4 h. Of this supernatant, 50 μL was transferred onto HEK-Blue IL-1β reporter cells (75×10^3) plated at a density of 0.5×10^6 cells/mL and incubated for 15 h following which SEAP activity in the HEK-Blue supernatant was measured using Quanti Blue reagent according to the manufacturer's protocol. The SEAP activity corresponds to the amount IL-1β secreted by THP-1 cells. Recombinant human IL-1β standards were used for comparison. The IL-1β activity was further confirmed by admixing antihuman IL-1β antibody (1 μg/mL) to the THP-1 supernatants prior to addition to HEK-Blue IL-1β cells. Activity was observed to drop to background levels (data not shown). Studies with THP-1shscr, THP-1shasc, and THP-1shcasp1 were performed similarly. Inhibitors isoliquiritigenin, MCC950, (5Z)-7-Oxozeaenol, takinib, E 64d, and Ca-074-Me were preincubated with cells for 30 min at a concentration of 30, 1, 10, 10, 10, and 20 μM, respectively, prior to the addition of the polymers. Each experiment was performed thrice independently with three replicates for each experiment.

Bone-Marrow-Derived Dendritic Cell Harvest and Culture. Bone-marrow-derived dendritic cells (BMDCs) were harvested from 6-week-old C57Bl/6J mice and B6.129S6-Nlrp3^{tm1Bhk}/J mice (Jackson Laboratory) following previous literature protocol.[35] On day 5, BMDCs were released and plated on 96-well plates at a density of 1×10^6 cells/mL (180 μL) and treated with ultrapure LPS (100 EU/mL) for 3 h following which the supernatant was removed, and cells were supplemented with fresh media and treated with LR+, LR−, or

DOI: 10.1021/acscentsci.8b00218
ACS Cent. Sci. 2018, 4, 982−995

TAT peptides for 4 h. The supernatant was diluted 2-fold and analyzed for IL-1β using ELISA. The experiment was performed twice independently with three replicates for each experiment.

Antibody Staining for ASC. Staining for ASC was performed on 3.7% formaldehyde-fixed THP-1 cells using rabbit polyclonal anti-TMS1 primary antibody and donkey antirabbit IgG Alexa Fluor 647 secondary antibody following conventional antibody staining protocols with cell permeabilization using 0.1% Triton X-100 and treatment with 0.01% Tween-20 to reduce background staining.

Confocal Microscopy. Fluorescent images were obtained on a LSM 700 or 780 confocal microscope (Zeiss) using Zen software. The following parameters were primarily used during image acquisition: scan speed 6, average of 4 scans, 1 Airy unit, and 1024 × 1024 μm/pixel resolution. A quantity of 20 μg of the polymers was used in potassium efflux experiments (Figure 8) compared to 8 μg in most other experiments for the ease of documenting a more defined change over time using microscopy techniques. Each microscopy experiment was performed twice independently with at least two replicates for each time point. At least 5 different regions were analyzed for each sample to obtain a representative image.

Image Processing. Image processing was performed using Zen software. Membrane compromised, pyroptotic cells were consistently observed to stain more intensely with Hoechst 33342. The intensity of nuclear stain has been adjusted in the images for better visual comparison.

ImageStream. Cell samples were analyzed on an Amnis ImageStream Mark II imaging flow cytometer with accompanying INSPIRE software. Sample images were acquired for 10 000 events and then analyzed using Amnis IDEAS v6.1 software. Color correction samples containing cells stained only with one fluorescent dye were run without brightfield and side scatter channel data collection to generate accurate fluorescence intensities for each channel. Cells were gated using the gradient RMS feature following which the population was gated for single cells. A quantity of 20 μg of the polymers was used in potassium efflux experiments (Figure 8) compared to 8 μg in most other experiments for the ease of documenting a more defined change over time. ImageStream experiments were performed twice independently with two replicates for each time point.

Flow Cytometry. Flow cytometry analysis was performed on an ACEA Novocyte flow cytometer. THP-1 cells (1.08×10^6) were plated in 24-well plates at a density of 2.0×10^6 cells/mL and treated with ultrapure LPS for 3 h. Following this the cells were washed and incubated with PBS with or without inhibitors (monensin, 2 μM; ammonium chloride, 25 mM; filipin-III, 30 μg/mL). Following this, the cells were incubated either with LR+/Fl or with LR+ for 4 h. Samples treated with LR+ were also incubated with Lysoview 633 for 30 min. The rate of endocytosis was assessed by measuring the median intensity of Alexa Fluor 488 while lysosomal rupture was assessed by analyzing the median intensity of Lysoview 633. The experiment was performed thrice independently with three replicates for each experiment.

Synthesis of TAT Peptides. Fmoc-solid phase peptide synthesis was performed using a CEM Liberty Blue peptide synthesizer using Rink amide resin (100−200 mesh) as the solid support. The N-terminus of the peptides was capped with azidohexanoic acid. Double coupling and extended coupling times were used to couple the arginines and the hexaethylene glycol linker. Peptides were deprotected using a mixture of 85% TFA mixed with 5% water, 5% anisole, and 5% thioanisole. Following this, they were precipitated in cold diethyl ether. The crude peptides were purified using a Phonomenex Luna C18 column (5 μm, 100 Å, 150 × 21.2 mm) on a Gilson preparative HPLC using a gradient of 25−45% acetonitrile (containing 0.1% TFA) in water (containing 0.1% TFA) over a period of 15 min at a flow rate of 21.2 mL/min. The purified peptides were lyophilized and characterized using MALDI-MS (see the Supporting Information).

Dynamic Light Scattering. Dynamic light scattering (DLS) measurements were performed by a Wyatt Mobius DLS instrument. Before the analysis or mixing with DQ BSA, the polymer solution was filtered through a 0.22 μm celltreat nylon membrane filter to remove particulates. Measurements were performed at 25 °C using a laser wavelength of 532 nm. Scattered light was collected at a fixed angle of 163.5°. The size distribution plots were obtained using the installed software from the instrument.

■ ASSOCIATED CONTENT

Supporting Information

The Supporting Information is available free of charge on the ACS Publications website at DOI: 10.1021/acscentsci.8b00218.

Characterization of the polymers and peptides, DLS characterization of biophysical properties of the polymers and DQ Green BSA conjugates, additional experimental details on DQ Green BSA experiment, incubation of polymers with FITC-dextran, and ROS production by polymers (PDF)

■ AUTHOR INFORMATION

Corresponding Author

*E-mail: aesserkahn@uchicago.edu.

ORCID

Zhibin Guan: 0000-0003-1370-1511

Aaron P. Esser-Kahn: 0000-0003-1273-0951

Author Contributions

‖S.M. and W.J.H. contributed equally. The manuscript was written through contributions of all authors. All authors have given approval to the final version of the manuscript.

Funding

This research was supported by Grants (7DP2Al112194-02), (5U01AI124286-02), and (R01DK098446) from NIH and (DMR-1609946) from NSF.

Notes

The authors declare no competing financial interest.

■ ACKNOWLEDGMENTS

We would like to thank Dr. Adeela Syed from the Optical Biology Core Facility at UCI and Dr. Vytas Bindokas from the Integrated Light Microscopy Core Facility at U Chicago for assistance with confocal microscopy. We would also like to thank Dr. Jennifer Atwood at the Flow Cytometry Facility at UCI for assistance with ImageStream and flow cytometry analysis. We also thank Dr. Philip Griffin from the Soft Matter Characterization Facility at U Chicago for assistance with DLS.

DOI: 10.1021/acscentsci.8b00218
ACS Cent. Sci. 2018, 4, 982−995

■ ABBREVIATIONS

TLR, Toll-like receptor; NLRP, NACHT, LRR, and Pyrin domain-containing protein; AIM2, absent in melanoma 2; IL-1β, Interleukin 1 beta; IL-18, Interleukin 18; ASC, apoptosis-associated specklike protein containing a caspase recruitment domain; BMDC, bone-marrow-derived dendritic cells

■ REFERENCES

(1) Schroder, K.; Tschopp, J. The Inflammasomes. *Cell* **2010**, *140*, 821−832.

(2) Guo, H.; Callaway, J. B.; Ting, J.P.-Y. Inflammasomes: mechanism of action, role in disease, and therapeutics. *Nat. Med.* **2015**, *21*, 677−687.

(3) Lamkanfi, M.; Dixit, V. M. Modulation of Inflammasome pathways by Bacterial and Viral Pathogens. *J. Immunol.* **2011**, *187*, 597−602.

(4) Shaw, P. J.; McDermott, M. F.; Kanneganti, T.-D. Inflammasomes and autoimmunity. *Trends Mol. Med.* **2011**, *17*, 57−64.

(5) He, Y.; Hara, H.; Nunez, G. Mechanism and Regulation of NLRP3 Inflammasome Activation. *Trends Biochem. Sci.* **2016**, *41*, 1012−1021.

(6) Munoz-Planillo, R.; Kuffa, P.; Martinez-Colon, G.; Smith, B. L.; Rajendiran, T. M.; Nunez, G. K+ Efflux Is the Common Trigger of NLRP3 Inflammasome Activation by Bacterial Toxins and Particulate Matter. *Immunity* **2013**, *38*, 1142−1153.

(7) Mariathasan, S.; Weiss, D. S.; Newton, K.; McBride, J.; O'Rouke, K.; Roose-Girma, M.; Lee, W. P.; Weinrauch, Y.; Monach, D. M.; Dixit, V. M. Cryopyrin activates the inflammasome in response to toxins and ATP. *Nature* **2006**, *440*, 228−232.

(8) Hornung, V.; Bauernfeind, F.; Halle, A.; Samstad, E. O.; Kono, H.; Rock, K. L.; Fitzgerald, K. A.; Latz, E. Silica crystals and aluminum salts activate the NALP3 inflammasome through phagosomal destabilization. *Nat. Immunol.* **2008**, *9*, 847−856.

(9) Bruchard, M.; Mignot, G.; Derangere, V.; Chalmin, F.; Chevriaux, A.; Vegran, F.; Boireau, F.; Simon, B.; Ryffel, B.; Connat, J. L.; Kanellopoulos, J.; Martin, F.; Rebe, C.; Apetoh, L.; Ghiringhelli, F. Chemotherapy-triggered cathepsin B release in myeloid-derived suppressor cells activates the Nlrp3 inflammasome and promotes tumor growth. *Nat. Med.* **2013**, *19*, 57−64.

(10) Eisenbarth, S. C.; Colegio, O. R.; O'Connor, W.; Sutterwala, F. S.; Flavell, R. A. Crucial role for the Nalp3 inflammasome in the immunostimulatory properties of aluminium adjuvants. *Nature* **2008**, *453*, 1122−1126.

(11) Marty-Roix, R.; Vladimer, G. I.; Pouliot, K.; Weng, D.; Buglione-Corbett, R.; West, K.; MacMicking, J. D.; Chee, J. D.; Wang, S.; Lu, S.; Lien, E. Identification of QS-21 as an inflammasome-activating molecular component of saponin adjuvants. *J. Biol. Chem.* **2016**, *291*, 1123−1136.

(12) Larena, M.; Holmgren, J.; Lebens, M.; Terrinoni, M.; Lundgren, A. Cholera Toxin, and the Related Nontoxic Adjuvants mmCT and dmLT, Promote Human Th17 Responses via Cyclic AMP−Protein Kinase A and Inflammasome-Dependent IL-1 Signaling. *J. Immunol.* **2015**, *194*, 3829−3839.

(13) Pack, D. W.; Hoffman, A. S.; Pun, S.; Stayton, P. S. Design and development of polymers for gene delivery. *Nat. Rev. Drug Discovery* **2005**, *4*, 581−593.

(14) Yin, H.; Kanasty, R. L.; Eltoukhy, A. A.; Vegas, A. J.; Dorkin, J. R.; Anderson, D. G. Non-viral vectors for gene-based therapy. *Nat. Rev. Genet.* **2014**, *15*, 541−555.

(15) Fong, D.; Grégoire-Gélinas, P.; Cheng, A. P.; Mezheritsky, T.; Lavertu, M.; Sato, S.; Hoemann, C. D. Lysosomal rupture induced by structurally distinct chitosans either promotes a type 1 IFN response or activates the inflammasome in macrophages. *Biomaterials* **2017**, *129*, 127−138.

(16) Bueter, C. L.; Lee, C. K.; Wang, J. P.; Ostroff, G. R.; Specht, C. A.; Levitz, S. M. Spectrum and Mechanisms of Inflammasome Activation by Chitosan. *J. Immunol.* **2014**, *192*, 5943−5951.

(17) Elieh Ali Komi, D.; Sharma, L.; Cruz, C. S. D. Chitin and Its Effects on Inflammatory and Immune Responses. *Clin. Rev. Allergy Immunol.* **2017**, 1−11.

(18) Carroll, E. C.; Jin, L.; Mori, A.; Muñoz-Wolf, N.; Oleszycka, E.; Moran, H. B. T.; Mansouri, S.; McEntee, C. P.; Lambe, E.; Agger, E. M.; Andersen, P.; Cunningham, C.; Hertzog, P.; Fitzgerald, K. A.; Bowie, A. G.; Lavelle, E. C. The Vaccine Adjuvant Chitosan Promotes Cellular Immunity via DNA Sensor cGAS-STING-Dependent Induction of Type I Interferons. *Immunity* **2016**, *44*, 597−608.

(19) Zeng, H.; Little, H. C.; Tiambeng, T. N.; Williams, G. A.; Guan, Z. Multifunctional Dendronized Peptide Polymer Platform for Safe and Effective siRNA Delivery. *J. Am. Chem. Soc.* **2013**, *135*, 4962−4965.

(20) Oldenhuis, N. J.; Eldredge, A. C.; Burts, A. O.; Ryu, K. A.; Chung, J.; Johnson, M. E.; Guan, Z. G. Biodegradable Dendronized Polymers for Efficient mRNA Delivery. *ChemistrySelect* **2016**, *1*, 4413−4417.

(21) Behr, J.-P. The proton sponge: a trick to enter cells the viruses did not exploit. *Chimia* **1997**, *51*, 34−36.

(22) Honda, H.; Nagai, Y.; Matsunaga, T.; Okamoto, N.; Watanabe, Y.; Tsuneyama, K.; Hayashi, H.; Fujii, I.; Ikutani, M.; Hirai, Y.; Muraguchi, A.; Takatsu, K. Isoliquiritigenin is a potent inhibitor of NLRP3 inflammasome activation and diet-induced adipose tissue inflammation. *J. Leukocyte Biol.* **2014**, *96*, 1087−1100.

(23) Coll, R. C.; Robertson, A. A.; Chae, J. J.; Higgins, S. C.; Muñoz-Planillo, R.; Inserra, M. C.; Vetter, I.; Dungan, L. S.; Monks, B. G.; Stutz, A.; Croker, D. E.; Butler, M. S.; Haneklaus, M.; Sutton, C. E.; Núñez, G.; Latz, E.; Kastner, D. L.; Mills, K. H.; Masters, S. L.; Schroder, K.; Cooper, M. A.; O'Neill, L. A. A small-molecule inhibitor of the Nlrp3 inflammasome for the treatment of inflammatory diseases. *Nat. Med.* **2015**, *21*, 248−255.

(24) Fernandes-Alnemri, T.; Wu, J.; Yu, J. W.; Datta, P.; Miller, B.; Jankowski, W.; Rosenberg, S.; Zhang, J.; Alnemri, E. S. The pyroptosome: a supramolecular assembly of ASC dimers mediating inflammatory cell death via caspase-1 activation. *Cell Death Differ.* **2007**, *14*, 1590−1604.

(25) Lu, A.; Magupalli, V. G.; Ruan, J.; Yin, Q.; Atianand, M. K.; Vos, M. R.; Schröder, G. F.; Fitzgerald, K. A.; Wu, H.; Egelman, E. H. Unified Polymerization Mechanism for the Assembly of ASC-Dependent Inflammasomes. *Cell* **2014**, *156*, 1193−1206.

(26) Cai, X.; Chen, J.; Xu, H.; Liu, S.; Jiang, Q. X.; Halfmann, R.; Chen, Z. J. Prion-like Polymerization Underlies Signal Transduction in Antiviral Immune Defense and Inflammasome Activation. *Cell* **2014**, *156*, 1207−1222.

(27) Tschopp, J.; Schroder, K. NLRP3 inflammasome activation: the convergence of multiple signalling pathways on ROS production? *Nat. Rev. Immunol.* **2010**, *10*, 210−215.

(28) Orlowski, G. M.; Colbert, J. D.; Sharma, S.; Bogyo, M.; Robertson, S. A.; Rock, K. L. Multiple Cathepsins Promote Pro−LR−1β Synthesis and NLRP3-Mediated LR−1β Activation. *J. Immunol.* **2015**, *195*, 1685−1697.

(29) Okada, M.; Matsuzawa, A.; Yoshimura, A.; Ichijo, H. The lysosome rupture-activated TAK1-JNK pathway regulated Nlrp3 inflammasome activation. *J. Biol. Chem.* **2014**, *289*, 32926−32936.

(30) Totzke, J.; Gurbani, D.; Raphemot, R.; Hughes, P. F.; Bodoor, K.; Carlson, D. A.; Loiselle, D. R.; Bera, A. K.; Eibschutz, L. S.; Perkins, M. M.; Eubanks, A. L.; Campbell, P. L.; Fox, D. A.; Westover, K. D.; Haystead, T. A. J; Derbyshire, E. R. Takinib, a selective TAK1 inhibitor, broadens the therapeutic efficacy of TNF-α inhibition for cancer and autoimmune diseases. *Cell Chemical Biology* **2017**, *24*, 1029−1039.

(31) Zhou, R.; Yazdi, A. S.; Menu, P.; Tschopp, J. A role for mitochondria in NLRP3 inflammasome activation. *Nature* **2011**, *469*, 221−225.

(32) Lönn, P.; Kacsinta, A. D.; Cui, X. S.; Hamil, A. S.; Kaulich, M.; Gogoi, K.; Dowdy, S. F.Enhancing endosomal escape for intracellular delivery of macromolecular biologic therapeutics. *Sci. Rep.* **2016**, *6*, 32301.

DOI: 10.1021/acscentsci.8b00218
ACS Cent. Sci. 2018, 4, 982−995

(33) Wu, J. Y.; Gardner, B. H.; Murphy, C. I.; Seals, J. R.; Kensil, C. R.; Recchia, J.; Beltz, G. A.; Newman, G. W.; Newman, M. J. Saponin adjuvant enhancement of antigen-specific immune responses to an experimental HIV-1 vaccine. *J. Immunol.* **1992**, *148* (5), 1519−1525.
(34) Gov, L.; Karimzadeh, A.; Ueno, N.; Lodoen, M. B. Human Innate Immunity to Toxoplasma gondii Is Mediated by Host Caspase-1 and ASC and Parasite GRA15. *mBio* **2013**, *4*, e00255-13.
(35) Tom, J. K.; Dostey, E. Y.; Wong, H. Y.; Stutts, L.; Moore, T.; Davies, H. W.; Felgner, P. L.; Esser-Kahn, A. P. Modulation of innate immune responses via covalently linked TLR agonists. *ACS Cent. Sci.* **2015**, *1*, 439−448.

DOI: 10.1021/acscentsci.8b00218
ACS Cent. Sci. 2018, 4, 982−995